Съгласен Юни
Нина Пенкова

До доц. д-р инж. Нина Пенкова
Ръководител на проект:
BG051PO001-3.3.06-0014:
“Център по математично моделиране и компютърна симулация за подготовка и развитие на млади изследователи”

ДОКЛАД
от

Николай Методиев Николов
/име, фамилия/
участник в целевата група по проекта

Уважаема г-жо Ръководител,

Бих желал да бъда информиран за възможността да бъде финансирано в общ размер от 22.56 лв. (двадесет и два лева и 56 ст.) доставянето на следните две научни статии :

```
Title: Cascade rubber dams fall discharge calculation and analysis,
AUTHOR(S): Zhang, Qinghua; Diao, Yanfang,
PUB. DATE: August 2011,
SOURCE: Canadian Journal of Civil Engineering; Aug2011, Vol. 38 Issue 8,p957;
Title:   Dynamic analysis of an inflatable dam subjected to a flood,
Authors: Lowery, K.; Liapis, S.,
Publication: Computational Mechanics, Volume 24, Issue 1, pp. 52-64 (1999).
(CompM Homepage);
```

свързани с работата ми по математическо моделиране и компютърна симулация на водонапълняеми хидротехнически мембранни конструкции.

Прилагам текста на кореспонденция с дирекция "НБИО" от НАЦИД с банковите реквизити за финансовия превод.

Дата: 28.02.2013 г. Подпис:

Веселин Илиев

From: V.Slavcheva [vs@nacid.bg]
Sent: 26 Август 2013 г. 09:24
To: Veselin Iliev
Subject: Re: NACID_zajvki

Добро утро,

Сумата е с ДДС. Съжалявам, че не го написах.

Поздрави,

Валентина Славчева

дирекция "НБИО"
НАЦИД

Здравейте,
Дали бихте уточнили сумата от 22.56 лв. с ДДС ли е или без ДДС.

Н. Николов

Уважаеми господин Николов,

Двете заявки за исканите от Вас статии са доставени в библиотеката.
Необходимо е да преведете по банковата сметка на НАЦИД следната сума:
3.00 лева за първата статия и 19.56 за втората.
Общата сума е 22.56 лв.
След получаването на сумата ще ви изпратя статиите.
За третата публикация трябва да изчакаме колежка, която ще се бъде на работа на 2.09.2013 г. Също така Ви моля да изпратите и данните за издаване на фактура за извършената услуга.

Банкови реквизити на НАЦИД :

BG97UNCR96603119995010

BIC: UNCRBGSF

УниКредит Булбанк

София

Изпълнените заявки:
Title: Cascade rubber dams fall discharge calculation and analysis
AUTHOR(S): Zhang, Qinghua; Diao, Yanfang
PUB. DATE: August 2011
SOURCE: Canadian Journal of Civil Engineering; Aug2011, Vol. 38 Issue 8, p957

Title:
Dynamic analysis of an inflatable dam subjected to a flood
Authors:
Lowery, K.; Liapis, S.
Publication:
Computational Mechanics, Volume 24, Issue 1, pp. 52-64 (1999). (CompM Homepage)

Поздрави,

Валентина Славчева
дирекция "НБИО"
НАЦИД

27.8.2013 г.

Computational Mechanics 24 (1999) 52–64 © Springer-Verlag 1999

Dynamic analysis of an inflatable dam subjected to a flood

K. Lowery, S. Liapis

Abstract A dynamic simulation of the response of an inflatable dam subjected to a flood is carried out to determine the survivability envelope of the dam where it can operate without rupture, or overflow. The free-surface flow problem is solved in two dimensions using a fully nonlinear mixed Eulerian-Lagrangian formulation. The dam is modeled as an elastic shell inflated with air and simply supported from two points. The finite element method is employed to determine the dynamic response of the structure using ABAQUS with a shell element. The problem is solved in the time domain which allows the prediction of a number of transient phenomena such as the generation of upstream advancing waves, the dynamic structural response and structural failure. Failure takes place when the dam either ruptures or overflows. Stresses in the dam material were monitored to determine when rupture occurs. An iterative study was performed to find the serviceability envelope of the dam in terms of the internal pressure and the flood Froude number for two flood depths. It was found that existing inflatable dams are quite effective in suppressing floods for a relatively wide range of flood velocities.

Symbols

h, d	The initial upstream water height (depth)
L	Tank length for the fluid solution
$\mathrm{Fn} \equiv U_B/\sqrt{g \cdot h}$	Froude number (non-dimensional velocity)
U_B	Upstream velocity (towing velocity)
R	Semi-circular obstruction height (radius)
g	The acceleration due to gravity
ρ	Density of water
$\alpha \equiv \frac{R}{h}$	Non-dimensional dam or obstruction height
t	Time
ϕ	The velocity potential
ψ	The stream function
∇	The gradient operator
D/Dt	The substantial derivative
x, y	The x and y Cartesian coordinates of a point
n	The unit normal to a surface
n_1	The x component of the unit normal to a surface
n_2	The y component of the unit normal to a surface
i	The imaginary number given by $\sqrt{(-1)}$ or an integer depending on context
$z = x + \mathrm{i}y$	The complex coordinate
$\beta = \phi + \mathrm{i}\psi$	The complex potential
Γ	Influence coefficient
L_d	Desingularization distance
π	The value for Pi (3.141592654...)
c	The local wave velocity
P	Pressure
η	Free surface elevation
θ	Angle varying from zero on the leading edge to π on the trailing edge of the obstruction
$C_p = P/\rho g h$	Pressure coefficient
$C_d = \mathrm{drag}/\rho g h^2$	Drag coefficient
$C_l = \mathrm{lift}/\rho g h^2$	Lift coefficient
PE	Potential energy
KE	Kinetic energy

1 Introduction

Inflatable dams are cylindrical in shape and attached to a foundation strip. They can be inflated with air, filled with water, or pressurized with a combination of air and water. Their height can be up to six meters and their length up to one hundred fifty meters. They may be anchored to a specifically made reinforced-concrete foundation strip or an existing base, like the crest of a dam. They are usually constructed of a nylon reinforced polymer. Inflatable dams are relatively easy to install, do not corrode, require little maintenance, and can handle extreme temperatures. They can be covered with impact resistant tiles to prevent them from being punctured by gunfire and other debris.

K. Lowery
Aker Engineering, 11757 Katy Freeway,
Suite 1300, Houston, TX 77079

S. Liapis ( )
Offshore Structures, Shell Oil Company,
3737 Bellaire Blvd, Houston, TX 77001

Most of this research was carried out while both authors were at Virginia Polytechnic Institute and State University. It was partially supported by a grant from the National Science Foundation (grant no. CMS-9422248). Thanks are due to Professor R.H. Plaut for many helpful comments.

Inflatable dams are currently used in a number of water control applications. These flexible structures may be used to temporarily store water or serve as dykes. In permanent applications, they can be used to direct water in irrigation, control water level in a hydroelectric facility, or raise the height of an existing dam. Several thousand inflatable dams are in use today. A 640-meter long string of seven inflatable dams is in place on the Susquehanna River in Pennsylvania to create Lake Augusta. Each segment is connected by concrete pylons to create a continuous dam. Some of the flow in the Santa Ana River in California is diverted by an inflatable dam to recharge groundwater. A large project to create a 220 surface-acre (850 feet wide by 2 miles long) lake in Tempe Arizona using inflatable dams is currently underway. Figure 1 shows an artist's rendition of this project. The city will construct a string of many 240 feet long inflatable dam sections ranging from six to sixteen feet in diameter. A one-inch wall thickness will be used over the entire dam. It is interesting to note that one section of the dam will be allowed to overflow at a controlled rate to produce a scenic cascade. Water will then be pumped back into to the lake to prevent runoff. The total construction cost of the dam is estimated to be forty million dollars. Many other examples of successful dams can be found worldwide. A few inflatable dams have failed during service. The Mangla Dam in Pakistan (see Binnie et al. 1973), became dynamically unstable and failed under overflow conditions.

Currently, inflatable dams are not used to suppress floods in emergencies. It is desirable to extend their use for this purpose. These dams could be placed along river banks to protect homes, businesses, industries, and towns from flooding. They could be deflated when not needed, to provide access and views, and then inflated when flooding is imminent. This requires some research to predict the dynamic response of the structure to flood conditions which is the objective of the present study.

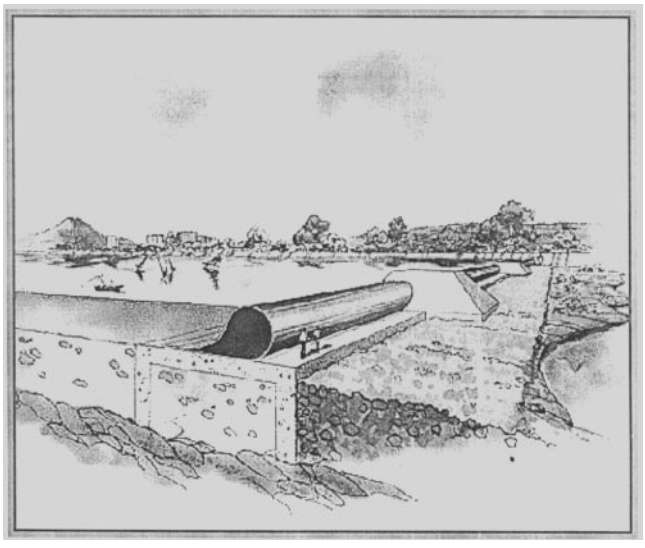

Fig. 1. Artist's rendition of the inflatable dam built to create a 220 surface-acre man made lake in Tempe, Arizona

Several authors have reported analytical results on inflatable dams. For example, Hsieh and Plaut (1990), and Al-Brahim (1994) analyzed the free vibrations of inflatable dams in two dimensions while Dakshina-Moorthy et al. (1995) and Mysore et al. (1998) studied free, three-dimensional vibrations of inflatable dams. Alwan (1986, 1988) performed modal analysis of an inflatable dam subjected to a flood. Wu and Plaut (1996) analyzed small vibrations of an inflatable dam under overflow conditions.

Also related to the present work, are studies of the dynamic characteristics of structures in air or in contact with water which have been carried out for a number of different practical applications. Kjellgren and Hyvarinen (1998) used a finite element numerical solution of the Navier-Stokes equations to compute the flow around moving structures such as sports car sections in two dimensions. Experimental data as well as numerical predictions of the natural frequencies and mode shapes of a flexible cylinder vibrating in air and in water were presented by Ergin et al. (1992). The dynamic response of a offshore platform subjected to random forces from waves was analyzed by Venkataramana and Kawano (1996). In a recent study, Nawrotzki et al. (1998) analyzed the elastic and inelastic response of shells using incremental path-following algorithms.

In this study, a dynamic simulation of the response of an inflatable dam subjected to a flood is carried out. Unlike the previous studies which solved the problem in the frequency domain, in the present work a fully nonlinear time-domain analysis is used. This allows for the prediction of large unsteady motions of the dam including cases where the dam ruptures or overflow occurs.

The problem of a flood impinging on an inflatable dam is assumed to be two-dimensional. In this study, a flood is taken to be a uniform stream of water striking the dam. The flood is assumed to start with a uniform depth of 2.0 or 3.0 meters, and a uniform velocity. The flow a sufficient distance ahead of the dam retains this initial velocity and depth. The analysis begins when the front of the flood is completely in contact with the dam.

The dam is anchored to the bottom at two points using pinned boundary conditions. Its stress free shape (initial shape) is that of a large semicircle. The dam has a uniform thickness and is comprised of nylon reinforced rubber. The dimensions and material properties of the structure used in the present study are representative of existing structures. Figure 2 illustrates the design of a typical inflatable dam. The dam is supported by an applied internal pressure ranging from a pressure of 1.0 to 5.0 meters of water. This internal pressure provides most of the stiffness required to repel a uniform flood applied to one side of the dam.

This problem has two distinct parts: nonlinear free-surface flow, and elastic structural dynamics. These two problems are coupled and must be solved simultaneously. Transient, fully nonlinear computations for the fluid flow are performed using a mixed Eulerian-Lagrangian formulation. The dam is modeled as an elastic shell inflated with air and simply supported from two points. The finite element method is employed to determine the dynamic response of the structure using ABAQUS with a shell

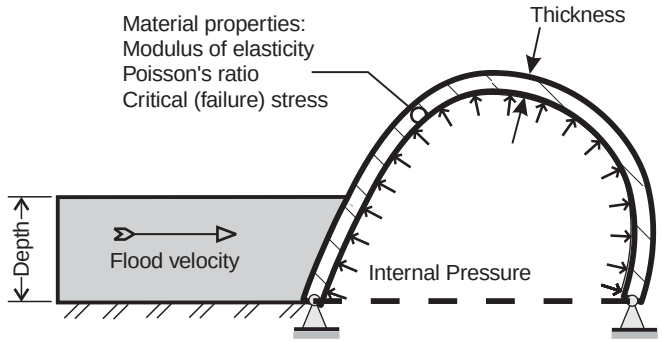

Fig. 2. Sketch of a typical inflatable dam illustrating some basic parameters influencing dam performance

element. A numerical towing tank with the inflatable dam on the downstream boundary and open boundary conditions on the upstream vertical boundary has been developed to simulate the fluid flow. The computer simulation "tows" the flexible dam at a steady Froude number. The fluid dynamics program determines the free-surface elevation and calculates the external pressure acting on the dam surface at each time step. This pressure is then used as an input by the ABAQUS model at each time step to determine the deformation and the velocities along the dam surface and the stresses in the dam. This information is used by the fluid dynamics program in the next time step to continue the dynamic analysis. The data for the response of the free surface is translated to a coordinate frame moving with the structure to show how the free surface develops over time.

The simulation was run over a range of Froude numbers to determine the internal pressures where the structure failed. Failure takes place when the dam either ruptures or overflows. Rupture is caused by too high an internal pressure. Overflow, on the other hand, is caused by too low an internal pressure, or too high a Froude number. Thus, a serviceability envelope is formed where the dam can operate safely. Two envelopes were developed corresponding to upstream flood depths of 2.0 and 3.0 meters.

The paper is organized as follows. Section 2 contains the mathematical formulation and numerical procedures for analyzing the fluid flow and the structural response. In Sect. 3 the numerical results for the fluid flow, the structural response and the operational envelope are presented. Concluding remarks are given in Sect. 4.

2
Fluid–structure interaction study

This problem can be separated into two parts at each time step. The fluid dynamic flow will be described first, followed by the structural analysis. The last section will describe how the solutions of these problems are coupled to produce the fully dynamic simulation.

2.1
Mathematical formulation of the fluid flow

The unsteady, two-dimensional potential flow of an inviscid, incompressible fluid induced by the motions of the flexible boundary, is analyzed. Under the usual assumptions of a two-dimensional, inviscid, irrotational flow, the problem may be described by a velocity potential, ϕ, and a stream function, ψ. The velocity potential, ϕ, is defined so that the fluid velocity vector is given by:

$$\vec{V} = \vec{\nabla}\phi$$

Instead of analyzing a uniform flow incident on the flexible structure, the interaction of an initially stationary fluid with a flexible structure moving to the left at a constant speed, U_B is considered. A stationary x-y coordinate system is used with y positive upwards and the x axis coinciding with the upper left corner of the undisturbed free surface.

The fluid domain is bounded by the free surface, the flexible boundary surface, the bottom and the far-field upstream boundary. Figure 3 shows the numerical tank layout. Non-dimensional variables are chosen such that the initial fluid depth, the acceleration of gravity and the fluid density are equal to one. The fluid flow solution is non-dimensionalized to allow easy application of various depths. The fluid flow problem may be described in terms of two non-dimensional parameters. A depth-based Froude number is defined as $\mathrm{Fn} \equiv U_B/\sqrt{g \cdot h}$, where U_B is the uniform upstream velocity, h is the uniform upstream depth, and g is the gravitational acceleration. The non-dimensional dam height is given as $\alpha \equiv \frac{R}{h}$ where R is the radius of the dam.

In the fluid domain R, the velocity potential ϕ, must satisfy the Laplace equation:

$$\nabla^2\phi = 0 \tag{1}$$

On the free surface, C_F, the kinematic boundary conditions are:

$$\frac{DX}{Dt} = \frac{\partial\phi}{\partial x} \quad \text{and} \quad \frac{DY}{Dt} = \frac{\partial\phi}{\partial y} \tag{2}$$

where X, Y are the x and y coordinates of the particle on the free surface. The dynamic free-surface condition is given by Bernoulli's equation:

$$\frac{D\phi}{Dt} = -\eta + \frac{(\nabla\phi)^2}{2} \tag{3}$$

where D is the substantial derivative, x and y are the coordinates of the position of a fluid particle, and η is the

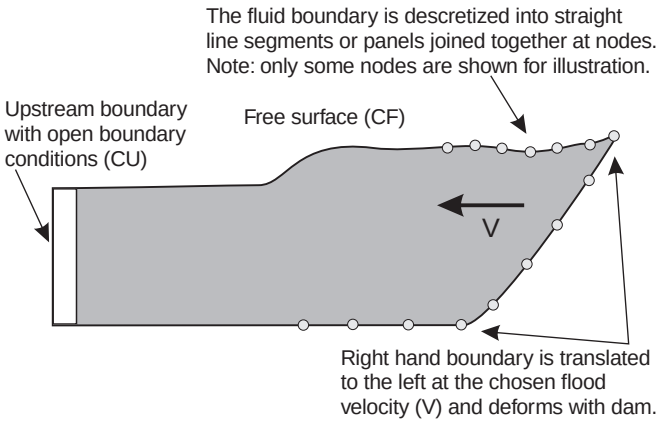

Fig. 3. Numerical towing tank layout

free surface elevation. On the flexible boundary surface, C_S, the fluid flow satisfies the no-penetration condition:

$$\frac{\partial \phi}{\partial n} = \frac{\partial \psi}{\partial s} = (u_d - U_B)\hat{n}_1 + v_d \hat{n}_2 \tag{4}$$

where U_B is the velocity of the boundary, s is the arclength along the boundary and n is the unit normal with components n_1 and n_2 in the x and y directions respectively. u_d and v_d are the components of the velocity of the flexible structure due to deformation in the x and y directions, respectively. On the flat bottom, C_B:

$$\frac{\partial \phi}{\partial n} = \frac{\partial \psi}{\partial s} = 0 \tag{5}$$

The complex coordinate is defined as $z = x + iy$, and the complex velocity potential, β, as $\beta(z) = \phi(z) + i\psi(z)$. Since β is analytic in the fluid domain, it satisfies Cauchy's integral theorem:

$$\oint_C \frac{\beta(z)}{(z - z_k)} dz$$

$$= \begin{cases} 0 & \text{for } z_k \text{ outside the fluid domain} \quad (6a) \\ -i\alpha_k \beta(z_k) & \text{for } z_k \text{ on the fluid boundary} \quad (6b) \\ 2\pi i \beta(z_k) & \text{for } z_k \text{ inside the fluid domain} \quad (6c) \end{cases}$$

where the contour C consists of the free surface, C_F, the bottom, C_B, the flexible boundary surface, C_S, and the upstream boundary. z_k is an arbitrary control point. The contour C is traversed such that the region R always lies to its left and α_k is the angle between two elements adjacent to z_k on the contour. For a smooth contour $\alpha_k = -\pi$.

A mixed Eulerian-Lagrangian (MEL) formulation is employed to solve the boundary value problem (1)–(5). This method has been used very successfully to predict a variety of nonlinear wave phenomena by a number of investigators (Longuet-Higgins and Cokelet 1976, Vinje and Brevig 1981, Lin 1984, Cointe 1989, Muthedath 1992). This method involves an Eulerian and a Lagrangian step. At each instant of time, the integral equation (6b) is solved numerically (Eulerian step). On some portions of the boundary φ is known (C_ϕ boundary) while on others ψ is known (C_ψ boundary). On the free surface φ is given by Eq. (3) while on the flat bottom ψ is zero and on the bottom obstacle surface ψ is given from Eq. (4). After solving the boundary value problem at each time step, the free surface conditions (2) and (3) are stepped forward in time to update the positions and the values of the velocity potential of particles of fixed identity (Lagrangian step). Only a brief description of the MEL formulation will be given here. More details may be found in Vinje and Brevig 1981 and Muthedath 1992.

2.1.1 Numerical implementation

The boundary C is divided into elements (panels). Figure 2 shows the layout of the tank and boundary elements. Within each panel, the complex potential, $\beta(z)$, is assumed to vary linearly with z. This can be expressed as:

$$\beta(z) = \frac{z - z_j}{z_{j-1} - z_j}\beta_{j-1} + \frac{z - z_{j-1}}{z_j - z_{j-1}}\beta_j \tag{7}$$

This approximation of $\beta(z)$ reduces the problem of finding a continuous potential to determining the unknown nodal values β_j. These are found by collocation, that is, by satisfying the integral Eq. (6) at the panel vertices. The result is a set of linear equations that can be solved for the unknown β_j^s. If Eq. (7) is substituted into Eq. (6a), a discretized form of the integral equation is found:

$$\oint_C \frac{\beta(z)}{(z - z_k)} dz = \sum_{j=1}^{N} \Gamma_{k,j}\beta_j = 0 \tag{8}$$

where the influence coefficients are given by:

$$\Gamma_{k,j} = \left\{\frac{z_k - z_{j-1}}{z_j - z_{j-1}}\right\} \ln\left\{\frac{z_j - z_k}{z_{j-1} - z_k}\right\} + \left\{\frac{z_k - z_{j+1}}{z_j - z_{j+1}}\right\} \ln\left\{\frac{z_{j+1} - z_k}{z_j - z_k}\right\} \tag{9}$$

z_j and z_k are the nodal and control point locations, respectively.

The fluid boundary consists of portions where ϕ is known (C_ϕ boundary) and portions where ψ is known (C_ψ boundary). At the free surface, the velocity potential ϕ is known (C_ϕ boundary) while on the bottom, the upstream boundary, and the flexible surface of the structure the stream function ψ is known (C_ψ boundary). The application of the boundary conditions is done by setting the appropriate terms in Eq. (8) to zero as follows:

$$\mathrm{Re}\left\{\sum_{j=1}^{N} \Gamma_{k,j}\beta_j\right\} = 0 \quad \text{for } z_k \text{ on } C_\phi \tag{10a}$$

$$\mathrm{Re}\left\{i\sum_{j=1}^{N} \Gamma_{k,j}\beta_j\right\} = 0 \quad \text{for } z_k \text{ on } C_\psi \tag{10b}$$

Special attention to the nodes at the intersection of the free surface with the upstream boundary and the surface of the structure is required. At these points, ϕ and ψ are completely known. No equation corresponding to ϕ or ψ on that point is used. This has been shown to be an effective treatment (see Lin 1984).

The flexible obstruction making up the right hand boundary is translated towards the left end of the tank to simulate flood conditions. Time stepping of Eqs. (2) and (3) is performed by Hamming's fourth order predictor/corrector method. A Runge-Kutta fourth order method is employed for the first four time steps to provide the initial starting data for use with Hamming's method. A non-dimensional time step of 0.05 seconds is used. The structure is started from rest with a velocity ramp. During this acceleration phase, the velocity is gradually increased in a linear fashion to its final value. It was found that a velocity increase of 0.05 Fn per time step provides a smooth startup.

Detailed accuracy and convergence tests were carried out to determine the numerical tank length, the panel arrangement and the time step size for the numerical simulations. Since the right boundary is moving to the left, the length, L of the numerical towing tank reduces with time. For the numerical results presented in this

study, the length of the tank was chosen equal to 40 times the fluid depth. This value of L was sufficient to provide the desired results before the computational domain became too short. A total of 509 nodes were used for the simulations presented here. 300 nodes were used on the free surface, 6 were used on the upstream boundary, 201 were used on the bottom boundary and 6 were used on the surface of the structure. This created 299, 5, 200, and 5 panels on the free surface, upstream boundary, bottom boundary, and structure surface, respectively. The nodes were spaced to provide uniform panel lengths on the computational boundary. Note that the panel lengths are not necessarily equal on the boundary segments.

2.1.2
Smoothing and node distribution on the free surface

Nodes on the free surface and the bottom boundary were redistributed at each time step to retain equal panel lengths on these boundaries as the tank length decreased.

Nodes on the free surface are smoothed every five time steps using a fifth order smoothing formula developed by Longuet-Higgins and Cokelet (1976)

$$\bar{y}_i = \tfrac{1}{16}(-y_{i-2} + 4y_{i-1} + 10y_i + 4y_{i+1} - y_{i+2}) \qquad (11)$$

where the subscript i indicates the ith node, $i-1$ is the previous node and so forth. Smoothing is necessary to suppress short wave, saw-tooth instabilities that are related to numerical error. This formula worked very well and suppressed all saw-tooth instability seen in this study. No adverse effects of smoothing such as introduction of numerical damping or dissipation to the numerical solution were observed.

2.1.3
Upstream boundary condition

A satisfactory treatment of the upstream boundary is of fundamental importance to the success of the numerical simulations. In this work, a Sommerfeld radiation condition is imposed at the upstream boundary in a manner similar to what has been used in other problems (Orlanski 1976). The following condition is imposed:

$$\frac{\partial \psi}{\partial t} + c\,\frac{\partial \psi}{\partial x} = 0 \qquad (12)$$

where c is the local wave velocity. This condition makes the upstream boundary transparent to all waves of velocity c, thus eliminating reflections. The local wave velocity, c is in the general case unknown. Some authors (Han et al. 1983) suggested a numerical method of calculating c. In the present study, c is set equal to the phase velocity $\sqrt{gh} = 1$ (unit depth and gravitational acceleration have been assumed). The numerical method used to apply Eq. (12) involves adding a column of points just inside the upstream and downstream boundaries. Then a finite difference scheme is employed to find the spatial and temporal derivatives of $\psi(z)$. For the time derivative, a backward difference scheme was used. For the spatial derivative, a forward difference scheme was used. This gives:

$$\frac{\psi(x_u, y_u, t) - \psi(x_u, y_u, t-\Delta t)}{\Delta t} + c\,\frac{\psi(x_u + \Delta x, y_u, t-\Delta t) - \psi(x_u, y_u, t-\Delta t)}{\Delta x} = 0 \qquad (13)$$

Rearranging to determine the nodal value of $\psi(x_u, y_u, t)$,

$$\psi(x_u, y_u, t) = \psi(x_u, y_u, t-\Delta t) - c\frac{\Delta t}{\Delta x}[\psi(x_u + \Delta x, y_u, t-\Delta t) - \psi(x_u, y_u, t-\Delta t)] \qquad (14)$$

where x_u, y_u is the coordinate of a node on the upstream boundary ($x_u = 0$), t is the current time in the simulation, Δt is the time step interval, and Δx is the distance of the additional points from the upstream boundary. The value of Δx used was 5 times the upstream depth. As usual, this optimum value for Δx was determined by trial and error. This scheme was tested, using both first and second order difference schemes to approximate the derivatives of $\psi(z)$, and various ways to determine the propagation velocity, c. The method shown and the simple choice of $c = 1$ was found to be superior and reduces the reflected waves to a minimum.

At each time step $(t - \Delta t)$ after solving for the value of ψ on the boundary nodes, the value of ψ on the interior points, $\psi(x_u + \Delta x, y_u, t - \Delta t)$ is determined using Eq. (6c). Then Eq. (14) is used to update the value of $\psi(x_u, y_u, t)$ at the nodes making up the upstream boundary at each time step.

2.1.4
Calculation of the pressure acting on the dam

The pressure over the surface of the structure is found using Bernoulli's equation:

$$P = \left[-\frac{\partial \varphi}{\partial t} - \frac{(\nabla \phi)^2}{2} - (y - \eta)\right] \qquad (15)$$

In order to evaluate the time derivative of the velocity potential, φ_t, we observe that the time derivative of the complex velocity potential, β_t, is analytic in the fluid domain. Therefore at each time step in a manner similar to the β problem, Eq. (6b) is solved for the unknown values of β_t. When solving for the time derivative β_t, on some of the boundaries φ_t is known while on others ψ_t is known , similar to the β problem. On the free surface φ_t is given by Eq. (3) as:

$$\frac{\partial \phi}{\partial t} = -\eta - \frac{(\nabla \phi)^2}{2}$$

On the far-field boundaries ψ_t is given from Eq. (12). On the flat bottom ψ_t is zero, while on the structure a divided difference formula is used to evaluate ψ_t.

2.2
Structural analysis

The dam is modeled as a thin elastic shell and is analyzed using the finite element method. The finite element package ABAQUS is used for both the static and dynamic

Table 1. Inflatable dam properties

	Property	Value
Dam design	Initial radius	4.5 m
	Initial thickness	1.27 cm
	Anchoring type	Double pinned
Material	Density	100 000 kg/sq m
	Poisson's ratio	0.45
	Modulus of elasticity	103.4 MPa
	Rupture stress	19.65 MPa

analysis. One hundred four-node thin shell elements (the S4R type described in the ABAQUS manual see Hibbitt et al. 1994) arranged along the circumference are employed. The elements have a uniform thickness of 1.27 cm and uniform material properties. The dam is anchored to the bottom at two points using pinned boundary conditions. Its stress free shape (initial shape) is that of a large semicircle. It is comprised of nylon reinforced rubber and has a uniform thickness of 1.27 cm. The dam is supported by an applied internal pressure ranging from a pressure of 1.0 to 5.0 meters of water. This internal pressure provides nearly all the stiffness required to repel a uniform flood applied to the one side of the dam. Table 1 contains the dimensions and material properties of the dam used in this study. These values are typical of existing structures.

The end points of the structure are anchored to the bottom using pinned boundary conditions. Since the problem is two-dimensional, the nodes are restrained from moving in the z direction. A uniform pressure is applied to the inside face of each element. The compressibility of the internal air was taken into account by assuming that it behaves isothermally. Hence, the internal pressure is not constant but is determined from the relation (pressure $\times$ volume) = c. The isothermal constant c is determined by taking the product of the initial prescribed pressure and the static volume of the dam. Then the value for the internal pressure at any point during the simulation may be found by dividing this constant by the new volume of the dam. The pressure caused by the effects of the external fluid (flood) is subtracted from the internal base pressure to obtain the pressure exerted on the dam. This pressure is distributed appropriately over elements making up the dam in the ABAQUS model.

2.3 Fluid–structure interaction

Values for the structural properties of the dam material, initial dam shape, the initial (base) internal dam pressure, the flood Froude number and the initial flood depth are input into a preprocessor. The preprocessor takes these values and creates the ABAQUS finite element model. Since the dam is initially started from rest, a static analysis must be performed first to determine the static shape of the dam produced by the influence of the external hydrostatic pressure and the internal inflation pressure. The hydrostatic pressure is found directly from the formula: $P_{stat} = \rho g d_{ave}$, where ρ is the density of water (1000 Kg/m^3), g is the gravitational acceleration (9.81 m/s^2), and d_{ave} is the average depth of each submerged element in the ABAQUS model. Figure 4 illustrates the application of the pressures on the structural model. The total pressure acting on each element is found by subtracting the static pressure, P_{stat}, from the internal pressure, P_{int}.

Once the static shape of the dam is found, the dynamic simulation is started. The translational velocity of the dam is smoothly started from rest to the final Froude number desired for each run. The two parts of the problem, the nonlinear free-surface flow and the structural deformation are coupled and must be solved simultaneously. The fluid flow depends on the structural deformation while the structural deformation depends on the fluid forces. There are many different methods for simulating such coupled fluid-structure interaction problems. In the present work, the fluid flow problem is solved first at each instant of time t. The new free surface shape, and the new pressure distribution acting on the dam are obtained. The total pressure acting on each element of the structure is found by subtracting the external pressure, P_{dyn} found by the fluids code from the isothermal internal pressure, P_{iso}:P_{tot} = P_{iso} P_{dyn}. The total pressure is used to create an ABAQUS restart file to perform a dynamic analysis over one time step. The ABAQUS dynamic analysis computes the stresses in the dam material as well as the new dam shape, and the velocity distribution for the next time step ($t + \Delta t$). After updating the shape of the structure, the new values of the stream function ψ are found by integrating Eq. (4) numerically. At the next time step ($t + \Delta t$) the entire procedure is repeated.

Figure 4 illustrates this method of solving the coupled fluid-structure interaction problem. More involved schemes to couple the fluid and structural solutions were considered such as iterating a few times between the two problems within each time step. The accuracy improvement using such schemes was found to be insignificant.

2.4 Failure criterion

Failure may occur in one of two ways, overflow and rupture. Overflow occurs when water flows over the dam. Rupture occurs when the breaking stress for the dam material is reached. The critical stress used here is 19.65 MPa. This stress is obtained by using a simple rule of mixtures to a rubber and nylon laminate (86% rubber, 14% nylon) typically used in the construction of inflatable dams.

2.4.1 Determination of the failure envelope

Failure is governed by three parameters: the internal dam pressure the flood depth and the flow Froude number. Two flood depths were chosen for this study, 2.0 and 3.0 meters. A serviceability envelope was produced for each depth. This envelope is the region of the internal pressure versus flood Froude number where the inflatable dam does not fail due to either overflow or rupture. A similar envelope could be developed for internal pressure versus flood depth, but was not done in this study.

The upper limit of the failure envelope corresponding to the internal pressure when the dam ruptures under

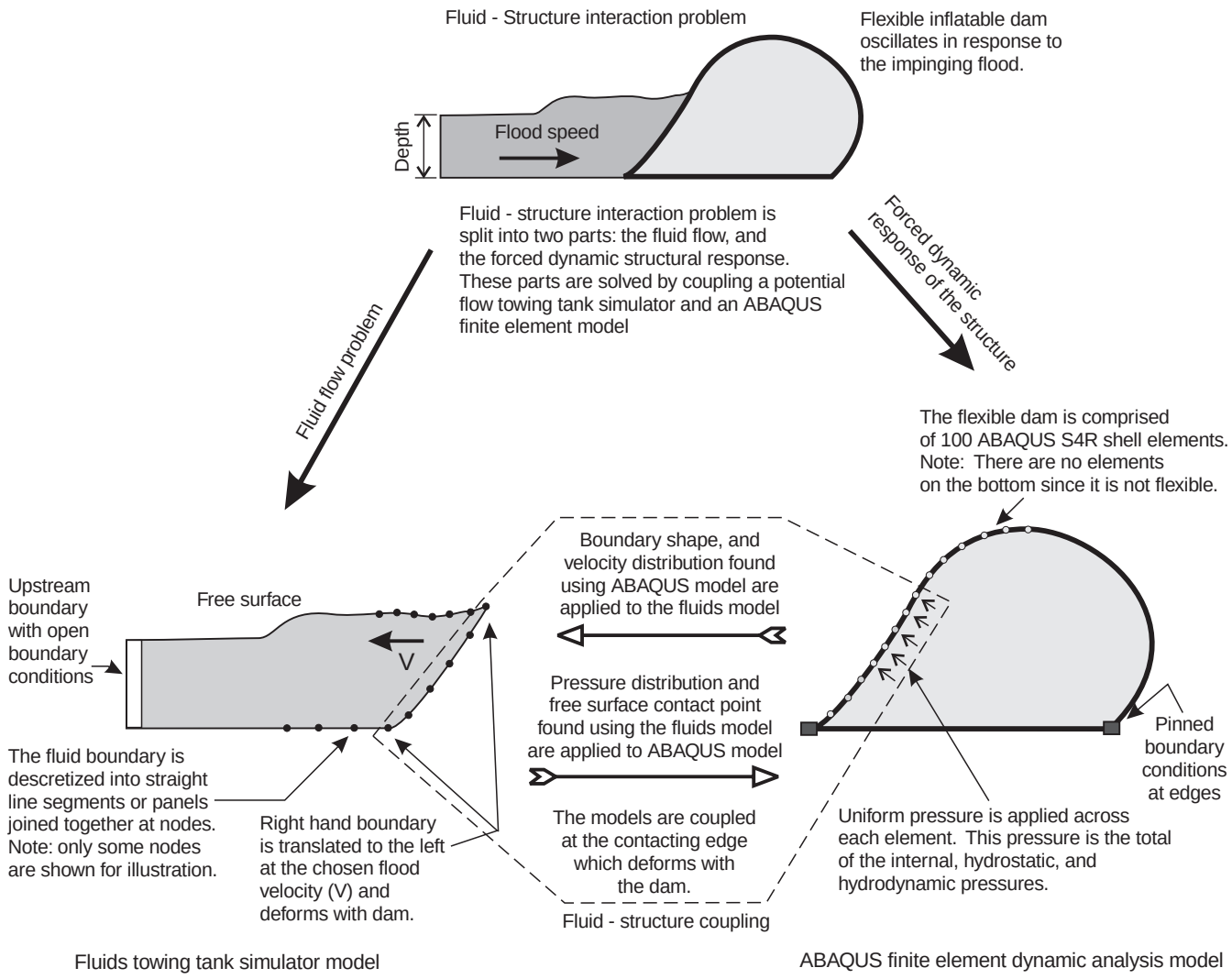

Fig. 4. Solving the fluid structure-interaction problem

hydrostatic pressures was found by iteratively running the static finite element model. Different values for the internal pressure were used until two values were obtained, one on each side of the rupture line, which only had a two percent difference. The lower limit of the failure envelope where the dam just overflows was found by running the full fluid structure interaction model in similar fashion as before while the Froude number was held at a fixed value. When the internal pressure required to suppress the flood exceeded the rupture value, the maximum flood Froude number sustainable had been reached, and the failure envelope was completely defined.

3
Numerical results

3.1
Fluid response

Figure 5 shows a sample displacement profile for a typical run in which the dam does not fail in overflow or rupture. As an alternative representation, Fig. 6 depicts the motion in a profile-temporal plot. As seen in these figures a bore of water is rejected to the left. Initially the flood pushes the dam to the right and subsequently the dam oscillates back and forth. This oscillation causes small waves to occur on top of the bore right next to the dam. As time progresses, the water height in front of the dam reaches a steady value. This height depends on the depth-based Froude number of the flood. The primary contribution to the forces exerted on the dam is from the hydrostatic pressure increase due to this increase in water level immediately in front of the dam.

Figure 7 is a sample free surface profile for a rigid dam illustrating the formation of a jet of water where the free surface contacts the dam. There is a jet of water produced when the flood first strikes the dam in the rigid case but not the flexible case. A jet occurs in many nonlinear free surface problems; see for example the water entry problem analyzed by Hughes (1973). The jet does not form in the case of a flexible dam since the structure deforms away from the jet and in a sense damps it out.

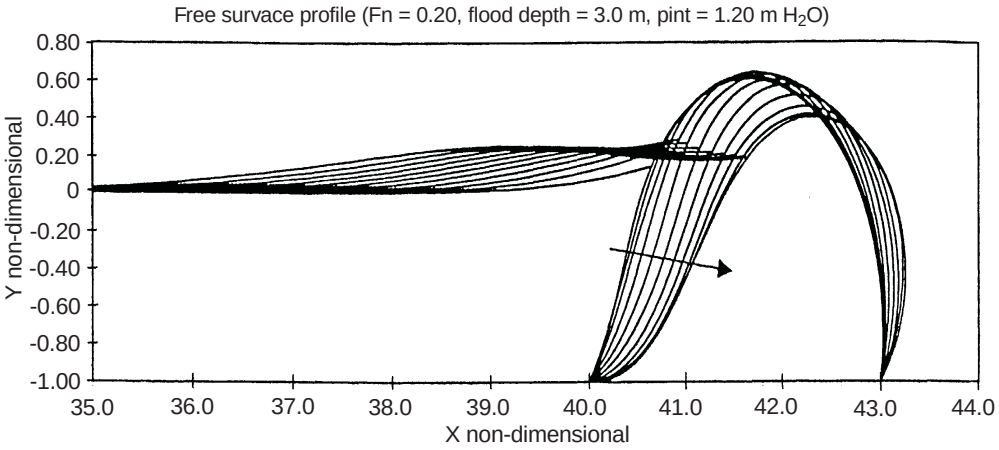

The flood in this plot is running from left to right. A sufficient distance from the dam it has a depth of 3.0 meters and Froude number (non-dimensional velocity) of 0.2. The dam is 4.5 meters tall and has an intemal pressure of 1.20 meters of water. After startup, the flood pushes the dam to the right. The floodwaters pile up in front of the dam and a left running bore of water is produced.

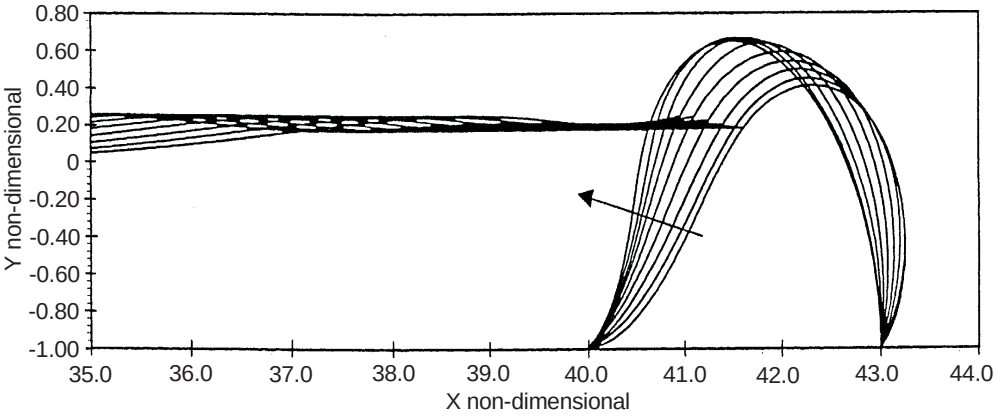

The dam, having receded too far "sling shots" back to the left. A small wave is produced on the free surface in front of the dam during this motion.

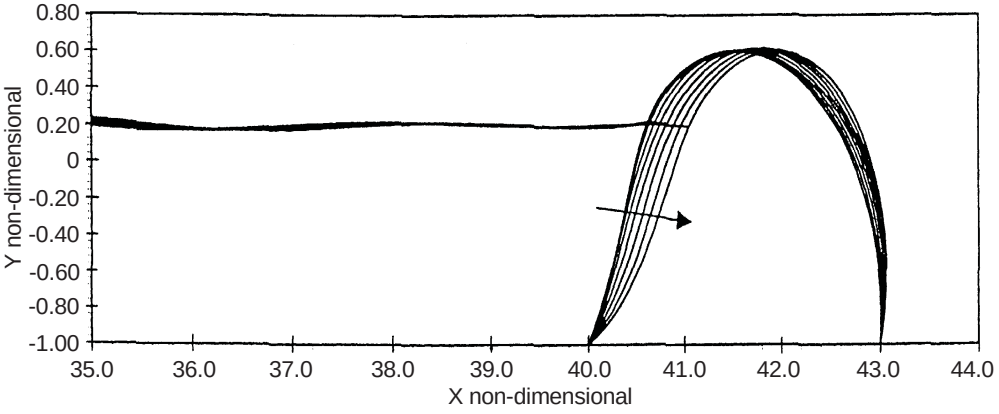

Having rebounded too far forward, the dam recedes once more. After a suffidently long time, the free surface in front of the dam reaches a steady height. Some low amplitude waves are generated during the oscillation of the dam in a similar fashion as a flap type wavemaker.

Fig. 5. Sample displacement profile for an inflatable dam in a flood

3.2 Structural response

3.2.1 Motion of the dam

Figures 5 and 6 show the motion of a dam for no overflow. As seen in the figure, the dam is pushed away from the flood and oscillates. The magnitude of the oscillations depends primarily on the internal pressure. As the internal pressure is increased, the oscillations decrease in magnitude, until they are hardly seen at all. At this point, the response of the flood closely resembles the results for the case of a rigid dam. A low pressure reduces the dam's ability to suppress the flood.

When the internal pressure is brought below a certain value, the dam can no longer hold back the flood, and overflow occurs. Figure 8 is a sample plot of an inflatable dam starting to overflow. Overflow is seen in this study as

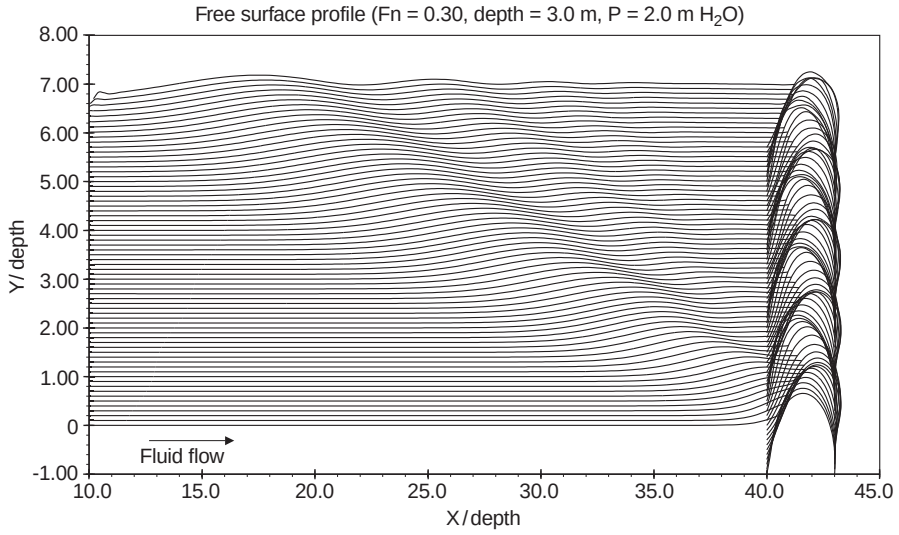

Fig. 6. Sample displacement – time profile plot of the free surface and an inflatable dam

the point where the thin region of water over the dam collapses. When this occurs, the nodes on the free surface and the dam touch and break down the numerical computations. The overflow pressure found here will be conservative as the dam may actually be barely able to contain the flood after the numerical computations break down.

Figure 9 is a plot of the trace of several nodes on the surface of the dam during a typical run. The node on the upstream side of the dam, at about the initial water level, displaces down and away from the flood, then returns on nearly the same path. The node on the top of the dam follows an orbital path such that it does not retrace its path as it "bounces back". The node on the downstream side of the dam displaces forward and backward on about the same path.

Figure 10 is a plot of the motion of the top node as a function of time. As seen in the plot, the motion in the x direction appears to be almost sinusoidal. For a flood depth of two meters, flood Froude number of 0.3, and an internal pressure of two meters of water, the period of this

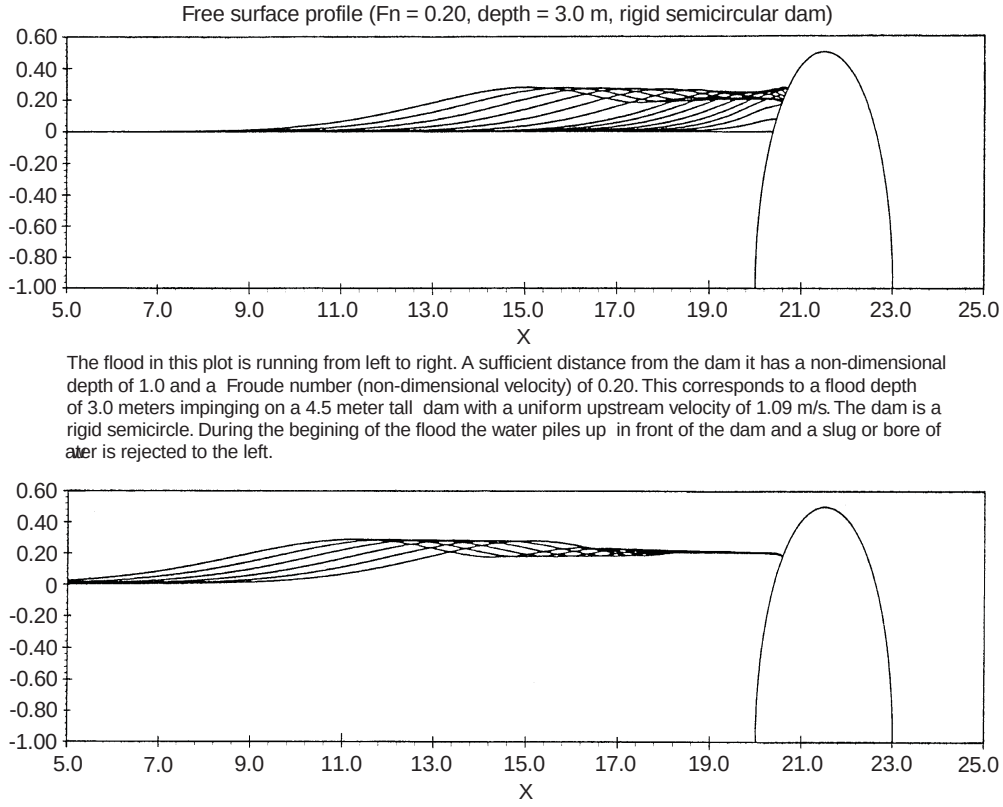

Fig. 7. Plot of the free surface response for a rigid dam

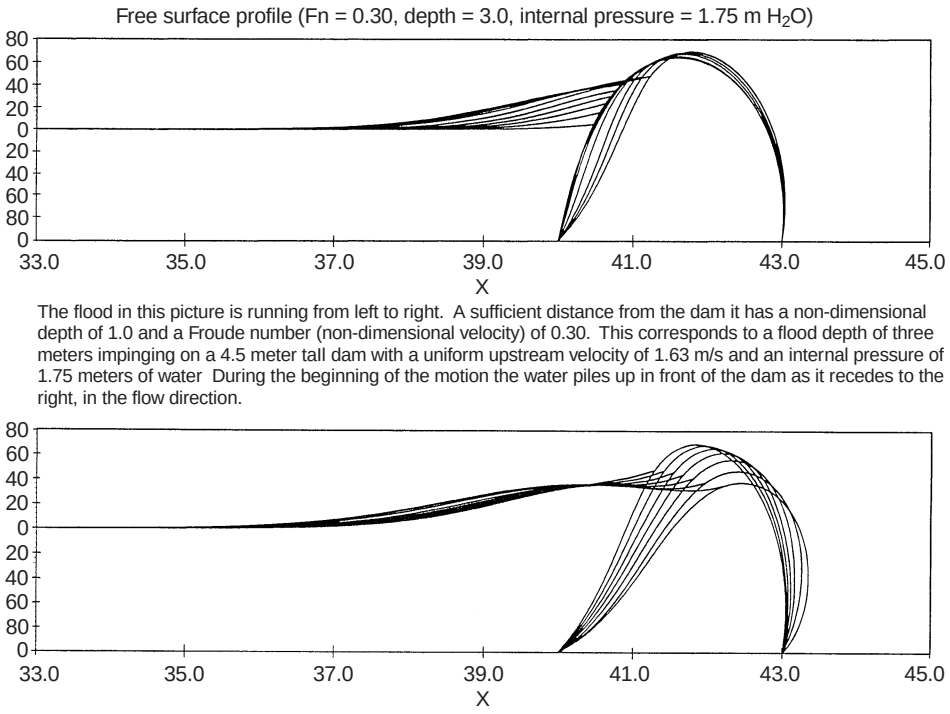

Fig. 8. Sample displacement profile for an inflatable dam during overflow

motion is roughly constant at about 0.377 seconds. The motion in the y direction is not as uniform. This shows that there is more than one mode being excited. The amplitude of the motion of a point on the dam is damped out during the run due to wave generation on the free surface.

3.2.2
Stresses in the dam

Figure 11 is a plot of the static stress (upstream flood speed = 0) in the dam for a low inflation pressure. The tensile stress is roughly constant over the surface of the dam. For an internal pressure of 1.75 meters of water, and a water depth of 3.0 meters the mean circumferential stress is 75 KPa. The mean transverse stress is 35 KPa. The maximum stress due to bending occurs about one meter from the bottom on the flood side of the dam. For this case, the maximum stress due to a combined state of bending and tension is about 340 KPa. For low pressures the bending stress is significant.

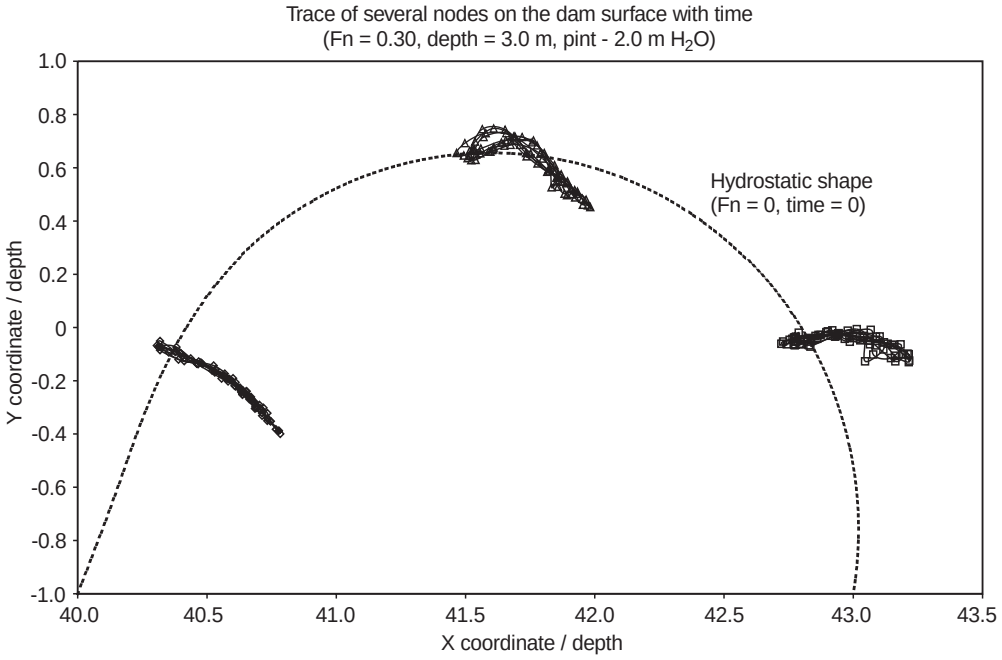

Fig. 9. Trace of several nodes on the surface of an oscillating inflatable dam

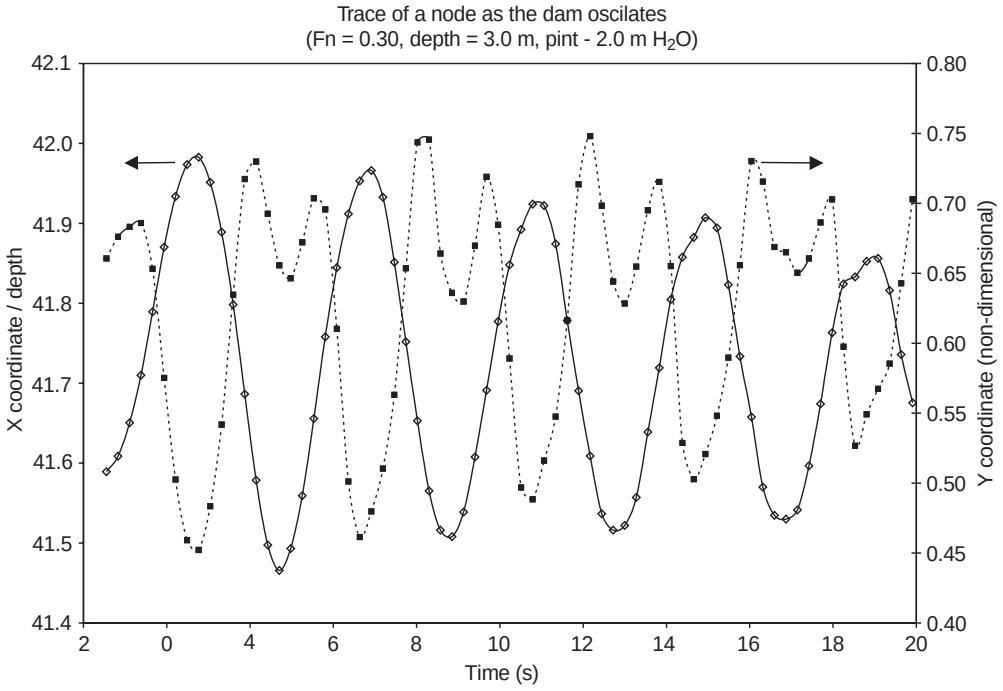

Fig. 10. The motion of the uppermost node of an oscillating inflatable dam as a function of time

Figure 12 is a plot of the static stresses in the dam for the rupture pressure in a 3.0 meter deep flood. For high pressures, closer to the rupture pressure, the bending stress is insignificant. For an internal pressure of 4.85 meters of water (the rupture pressure for this depth) and a water depth of 3.0 meters, the mean circumferential stress roughly equals the maximum stress (through the thickness). The mean circumferential stress is 19.5 MPa, and the mean transverse stress is 8.82 MPa.

Figure 13 contains sample results for the dynamic stress fluctuation with time at a node on the top of the dam. The stresses at other locations in the dam are qualitatively similar to this sample. It is an interesting to note that the flood actually lowers the stresses in the dam material. As Fig. 13 indicates, as time increases, the mean stress drops. As a result, the highest stress occurs near the beginning of the run, and the dynamic stress fluctuation is only about 10% of the total stress. Therefore, if the dam is going to rupture, it will most likely occur at the beginning under static loading. This may be explained by the fact that the water depth in front of the dam increases due to the flood. The increasing hydrostatic pressure outside the dam partially counteracts the pressure inside the dam. This results in decreased stresses in the dam.

3.2.3
The operational envelope

Figures 14 and 15 are plots of the serviceability regions for flood depths of two and three meters, respectively. A comparison of these two plots reveals that for a lower flood depth, a faster moving flood can be suppressed. In addition, the rupture pressure for a lower flood depth is

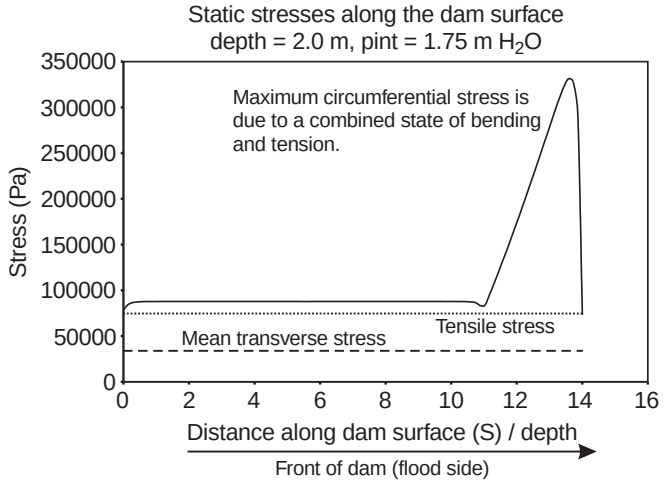

Fig. 11. Plot of the static stress in the dam for a low inflation pressure

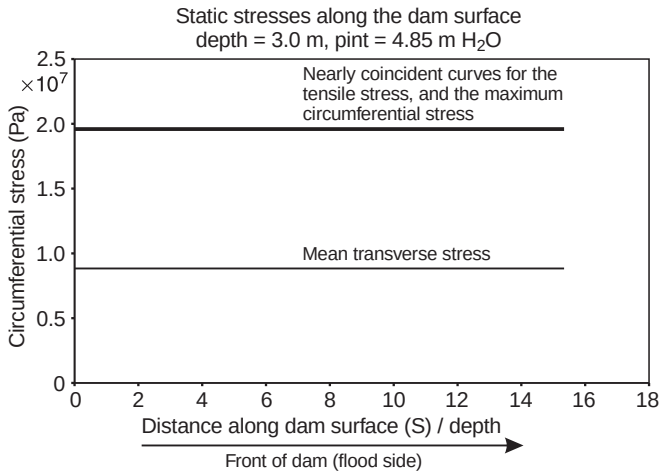

Fig. 12. Plot of the static stresses in the dam for an inflation pressure that would cause the dam to rupture

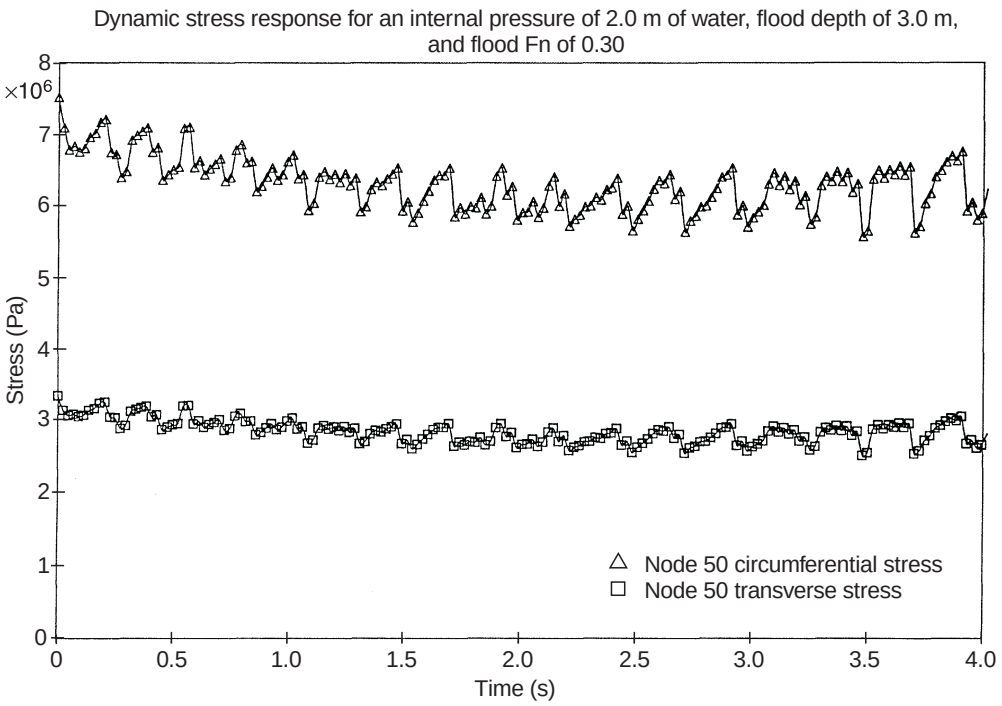

Fig. 13. Dynamic stresses at a point on the top of the dam

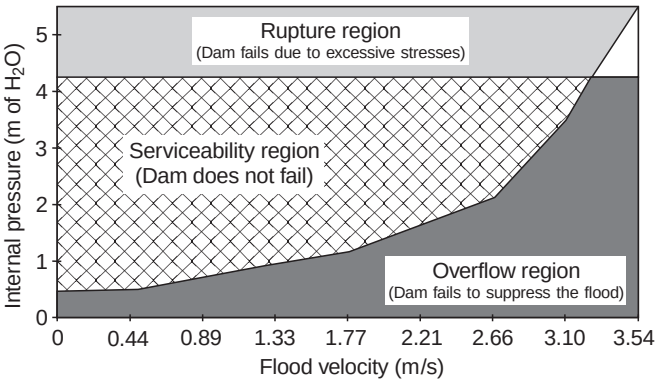

Fig. 14. Serviceability envelope for a flood depth of two meters

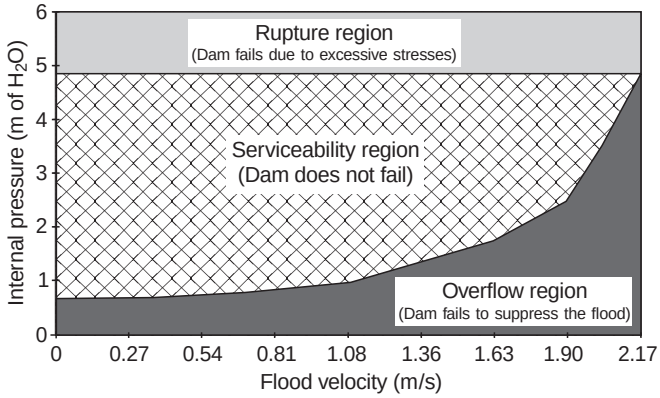

Fig. 15. Serviceability envelope for a flood depth of three meters

actually lower than that for a higher flood. This is due to the partial cancellation of external and internal pressures. A higher depth counteracts more of the applied internal pressure, and actually stabilizes the dam against rupture. From Figs. 14 and 15, it may be concluded that existing inflatable dams are quite effective in suppressing floods for a relatively wide range of flood velocities.

4 Conclusions

The effectiveness of a flexible inflatable dam to suppress floods in emergencies was studied numerically. Such structures have been used for water storage and irrigation but not to control floods. To this end, the dynamic, nonlinear response of an inflatable dam to a flood was studied for a range of flood depths and flood speeds. The numerical analysis was carried out in the time domain. A fully nonlinear Eulerian-Lagrangian formulation was used to simulate the fluid flow. The dam is modeled as an elastic shell inflated with air and simply supported from two points. The finite element method was employed to determine the dynamic response of the structure using ABAQUS with a shell element.

The dimensions and material properties of the structure used in the present study are representative of existing structures. No effort was made in the present work to vary the material properties and the dimensions of the structure and optimize the structural performance for a fixed cost. The serviceability regions for flood depths of two and three meters, respectively were obtained as functions of the internal pressure. If this pressure is too low, the water will overflow the dam. If it is too high, the dam will rupture. From Figs. 14 and 15, it may be concluded that existing inflatable dams are quite effective in suppressing floods for a relatively wide range of flood velocities.

References

Al-Brahim AM (1994) Free Vibration of Membrane Dams. European Earthquake Eng. 8

Alwan AD (1986) Modal analysis of inflatable dams under hydrodynamic conditions. Proc. 4th Intl Modal Analysis Conference, Los Angeles, California pp. 1502–1509

Alwan AD (1988) Modal analysis of flexible structures used for flood control. Proc. 6th Intl Modal Analysis Conference, Kissimmee, Florida pp. 1180–1185

Binnie GM, Thomas AR, Gwyther JR (1973) Inflatable weir used during construction of Mangala Dam. Proc. Instn. Civ, Engs, Part I 54

Cointe R (1989) Nonlinear simulation of transient free surface flows. Proceedings of the Fifth International Conference on numerical ship hydrodynamics, Hiroshima, Japan pp. 239–250

Dakshina Moorthy CM, Reddy JN, Plaut RH (1995) Three dimensional vibrations of inflatable dams. Thin-Walled Structures 21:291–306

Ergin A, Price WG, Randall R, Temarel P (1992) Dynamic characteristics of a submerged, flexible cylinder vibrating in finite water depths. J. Ship Res. 36(2):154–167

Han TY, Meng JCS, Innis GE (1983) An open boundary condition for incompressible stratified flows. J. Comput. Phys. 49:276–297

Hibbitt, Karlsson, Sorensen (1994) ABAQUS Theory Manual, Version 5.4, Pawtucket, RI

Hsieh JC, Plaut RH (1990) Free vibrations of Inflatable Dams. Acta. Mech. 85:207–220

Hughes OF (1973) Some characteristics in the free surface in the wedge entry problem. J. Eng. Math. 4:367–375

Kjellgren P, Hyvarinen J (1998) An arbitrary Lagrangian-Eulerian finite element method. Comput. Mech. 21:81–90

Lin WM (1984) Nonlinear motion of the free surface near a moving body. Ph.D. Thesis, Massachussets Institute of Technology, Cambridge, Mass

Longuet-Higgins MS, Cokelet ED (1976) The deformation of steep surface waves on water. Proc. R. Soc. Lond. A. 350: 1–26

Muthedath P (1992) Numerical study of nonlinear free surface flows. Ms. Thesis, Virginia Polytechnic Institute and State University, Blacksburg, VA

Mysore GV, Liapis SI, Plaut RH (1998) Dynamic analysis of single-anchor inflatable dams. J. Sound and Vibration 215(2):251–272

Nawrotzki P, Kratzig WB, Montag U (1998) Dynamic instability analysis of elastic and inelastic shells. Comput. Mech. 21:48–59

Orlanski I (1976) A simple boundary condition for unbounded hyperbolic flows. J. Comput. Phys. 21:251–269

Venkataramana K, Kawano K (1996) Parametric uncertainties for dynamic response evaluation of offshore structures. Comput. Mech. 18:454–463

Vinje T, Brevig P (1981) Breaking waves on finite water depths. A numerical study. The ship research institute of Norway

Wu PH, Plaut RH (1996) Analysis of the Vibrations of Inflatable Dams Under Overflow Conditions. Thin-Walled Structures 26(4)